Hindawi
Advances in Civil Engineering
Volume 2021, Article ID 5599925, 16 pages
https://doi.org/10.1155/2021/5599925

Research Article

Field Measurement and Numerical Modelling Study on Mining-Induced Subsidence in a Typical Underground Mining Area of Northwestern China

Kai Zhang,[1] Lu Bai,[1] Pengfei Wang ,[2,3] and Zhuang Zhu[2]

[1]*School of Chemical & Environmental Engineering, China University of Mining and Technology (Beijing), Beijing 100083, China*
[2]*College of Mining Engineering, Taiyuan University of Technology, Taiyuan, China*
[3]*Department of Mining, Metals and Materials Engineering, McGill University, Montreal, QC 3450, Canada*

Correspondence should be addressed to Pengfei Wang; 18801448768@163.com

Received 3 February 2021; Revised 1 April 2021; Accepted 7 April 2021; Published 26 April 2021

Academic Editor: Castorina S. Vieira

Mining-induced subsidence is a great concern for environmental protection in underground mining areas in China and all over the world. In view of the fact that the research on land degradation above underground coal mines are completely or partially independent of coal mining activity and the fact that the mechanism behind mining-induced subsidence has not been well understood, this study presents a field measurement and numerical study of mining-induced subsidence with respect to mining activity of three adjacent longwall panels in a coal mine in Northwest China. This study shows that surface subsidence lags far behind panel extraction or mining activity. The profiles of ground surface are dominated and manifested by the subsurface strata structures. The subsidence influence throughout the whole length of a longwall panel varies. Stability of strata structures within overburden before the final subsidence controls the stability of ground surface land. Chain pillars of 20 m between panels of 240 m wide with cover depth of 600 m have been crushed in the gob and do not have any function in supporting the overburden strata. The final subsidence of the three adjacent panels is far to come in the future and the land reuse above underground coal mines should be carefully planned by making sure that the gob is completely compacted or no potential secondary subsidence occurs in the future.

1. Introduction

There are many environmental issues associated with mining including air pollution due to dust and gas emission, water contamination, loss of groundwater resources, destruction to the surface structures, and degradation of ecosystems [1,2]. Underground mining, in particular, has a significant influence on ground movement or is known as subsidence, which induces serious environmental disturbances on land [3]. Many studies have been conducted on land degradation above underground coal mine workings such as water content change within the soil, evolution of physical and chemical properties of soil, and vegetation deterioration as shown in Figure 1.

In fact, back to the early days of the 1980s and 1990s in the US, the impact of mine subsidence on aquifer, farmland, agriculture, and other environmental issues had been studied [4–6]. Booth et al. [7] discussed the impact of mining on groundwater including decline and recovery of water levels. Utilizing a probability (frequency ratio) model, a statistical (logistic regression) model, and a Geographic Information System (GIS), [8] constructed a subsidence hazard map around abandoned underground coal mines at Samcheok City, Korea. Reference [9] conducted a comparison study on groundwater system before and after longwall mining with the condition of shallow cover depth. Using subsurface subsidence prediction model, Cheng et al. [10] carried out a study on strata deformation over longwall coal pillars. Marino et al. [11] presented an empirical approach for evaluating ground movement due to mining, which allows for realistic understanding of the historical and adverse subsidence-induced movements. Shi et al. [12]

Figure 1: Land degradation due to underground mining.

carried out a study on the influence of mining-induced subsidence on soil bacterial communities in aeolian sand area of western China. Marino et al. [13] proposed a high-accuracy method to identify the location of mining disturbances and the time when they occurred by analyzing Landsat data. Guney and Gal [14] reported a case study analysis of surface subsidence of a Turkey longwall mine under weak geological conditions. Ma et al. [15] presented a study of soil fertility decrease due to mining-induced subsidence in arid and semiarid regions. A finite element analysis was performed by Marian et al. [16] to study the state of stresses on the structures of buildings subjected to the impact of underground mining of hard coal seams in the Jiu Valley Basin (Romania).

As for the land destruction due to mining-induced subsidence, a number of studies on mitigation and reclamation of land have been carried out. Dawkins [17] discussed potential management and rehabilitation requirements of environmental effects from longwall subsidence on streams, lakes, and groundwater systems. Haibach et al. [18] provided some mitigation techniques to cope with the impacts of subsidence on streams. Hu et al. [19] presented a new reclamation technology, which is called concurrent mining and reclamation plans for yet-to-be-stable subsiding land against a case study mining area in northern Anhui province, China. Li et al. [20] carried out a comparative study of bacterial diversity of soils from mining subsidence and reclamation areas through pyrosequencing analysis. Based on replicated analysis across 18 mitigation sites, a study of the restoration of macroinvertebrates, fish, and habitats in streams following mining subsidence is presented by Tim et al. (2017). Wang et al. [21] carried out a study on separation and fracturing in overlying strata disturbed by longwall mining in a mineral deposit seam. Bi et al. [22] studied the alleviation of root damage stress induced by simulated coal mining subsidence ground fissures by arbuscular mycorrhizal fungi. In view of the significance of reclamation time in coal mining subsidence areas after mining, Wang et al. [23] revealed that fertilization can shorten the restoration time and reclamation time is crucial for the restoration of soil bacterial communities.

The mechanism behind land subsidence due to mining is in urgent need to take positive measures for environmental protection in the future mining which is good for homonymous development of mining industry and local environment. More appropriate measures are only able to be taken when the mechanism behind it is cleared. However, the above findings of surface subsidence or physical or chemical changes of soil and mining activity are completely or partially independent of each other; the relationship between these findings and mining activity has not been studied deeply or completely. In another word, the mechanism behind these findings has not been well understood. Instead of taking some positive measures, some passive measures are usually taken to protect associated hazards. And most importantly, those studies were mostly on large scale or in macrolevel. As a result, the accuracy and dimension of the above studies are hard to be adopted to guide land restoration and reclamation specifically and accordingly. As is known, the degree of damage of mining on land or soil cannot be evaluated precisely, because the damage degrees are different from region to region, mine to mine, panel to panel, and even patch to patch. For instance, subsidence changes the structure of the overlying strata; deformation of the surface above the panel center is different from that above the barrier pillars or chain pillars. The damage that topsoil suffered must be different; then, the vegetation restoration plan must be adjusted to those conditions, so as to reach better land protection or reclamation results. Therefore, this study presents a study of mining subsidence with respect to mining activity of three adjacent longwall panels in a coal mine in Northwest China in order to provide some insights which we hope can provide a reference for the land subsidence prediction and land rehabilitation measure selection.

2. Characteristics of the Study Area

The case study mine is located in the southernmost region of Wushen County, Ordos, Inner Mongolia, China, as shown in Figure 1. The mine is 63 km away from Wushen County government. The annual output of the mine is 8 million tons per year and the service life is 71 years. Elevation of the surface of the region is +1138.0 ~ +1125.1 m above sea level. The surface is mainly aeolian sand dune field dispersed with many stable and quasiflow crescent-shaped sand dunes. The natural vegetation consists of typically poplar trees. No important or large buildings or houses are there.

The mine is using a fully mechanized longwall mining method. The case study longwall panels are located in the southern-eastern part of the first miming district which is shown in Figure 2. The case study longwall panels are

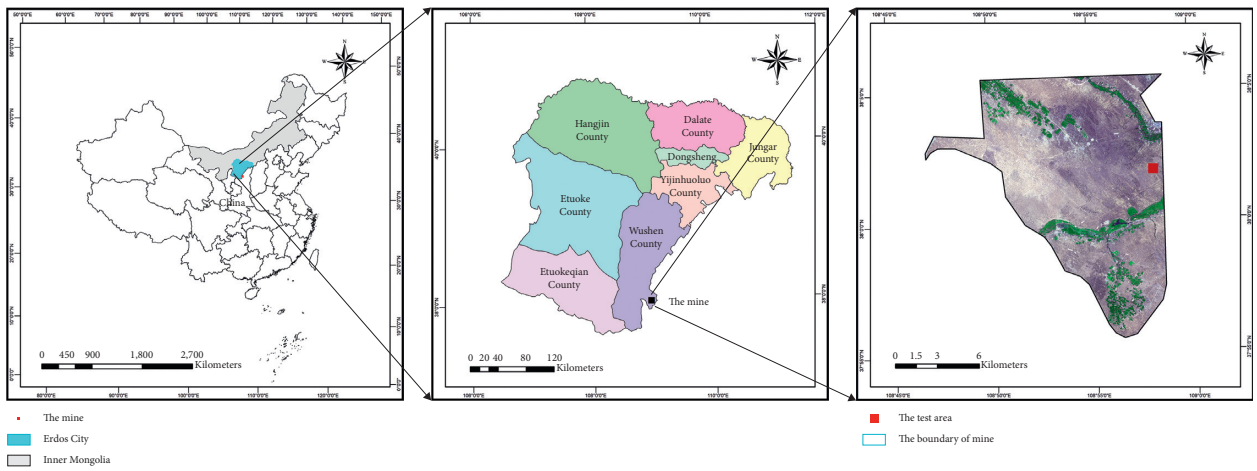

Figure 2: The location of the mine.

highlighted in red square. 31102 longwall panel is 241 m wide and 3100 m long. The minable area is 746618 m^2 with a total reserve of 5.23 million tons of coal. And 31103 longwall panel is 241 m wide and 3600 m long. The chain pillars between all the panels are all 20 m. The mining height of all panels is 5.5 m. The elevation of the coal seam is +571.898 ~ +585.136 m. In ascending order, the roof consists of sandy mudstone (20.1 m), fine-grained sandstone (13.6 m), and sandy mudstone (15.6 m). In descending order, the floor consists of sandy mudstone (15.3 m) and fine-grained sandstone (6.6 m) as shown in Figure 3. ZY13000/28/62D shields are used for roof support in the working face.

3. Field Measurement Instrumentation Plan

There are 4 monitoring lines above the case study longwall panels with one line across the three panels in the dip direction and two-line along the strike direction as shown in Figure 4.

Line N is in the middle of 31102 panel across the setup room and along the strike with a length of 1275 m. There are 50 points in total, which are numbered from N01 to N45 with a spacing of 25 m. Monitoring of this line started from Nov 21, 2017, to Oct 24, 2018.

Line A is in the middle of 31103 panel. 62 monitoring points are numbered AK1–AK3 and A1–A61; the data were collected from July 27, 2019, to July 5, 2020, with 22 groups of data. The invalid points include AK1, AK2, A1, A3, A7, A10, A11, A14, A21, A24, A54, and A56 due to weather or other reasons.

Line Q is along the dip of 31102 and 31103 panels. 73 points are numbered KQ1–KQ3, Q1–Q23, Z33, Q25–Q48, W1–W20, and K1–K3. As the measuring points were installed in the area where quicksand was prevailing, the data of points K1, K2, W16, W2, Q47, Q35, Q26-Q21, and Q18 were missing or partially missing. The details about the monitoring lines are given in Table 1.

For each point, a survey peg was mounted using C20 cement with steel reinforcement. The peg dimension is 0.5 m × 0.5 m × 2 m as shown in Figure 5. The buried depth of each peg is no less than 0.6 m. The number of each point is marked on the top of the peg. Then total stations are used to measure the displacement of each point.

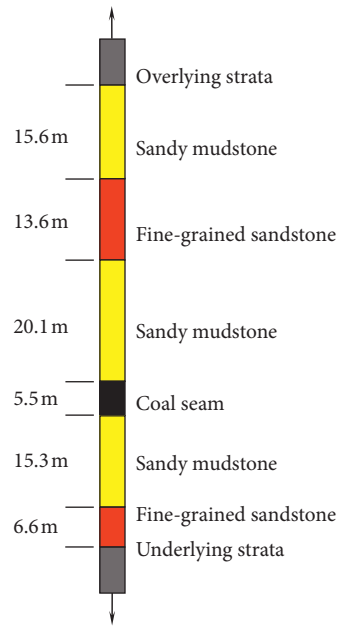

Figure 3: Generalized stratigraphy column.

During the early stage of panel extraction, monitoring was carried out comprehensively every month; at this stage, the surface subsidence rate was less than 50 mm/month. During the fast subsidence stage, 2-3-times of survey had to be carried out each month. For the later stage when the subsidence nearly ceased (less than 30 mm subsidence in a period of 6 months), 1-2 times of complete survey were required.

4. Field Measurement Data Analysis and Discussion

Survey for Line N was conducted 15 times from 11/16/2017 to 5/14/2019 as shown in Table 2. The profile of this line is shown in Figure 6.

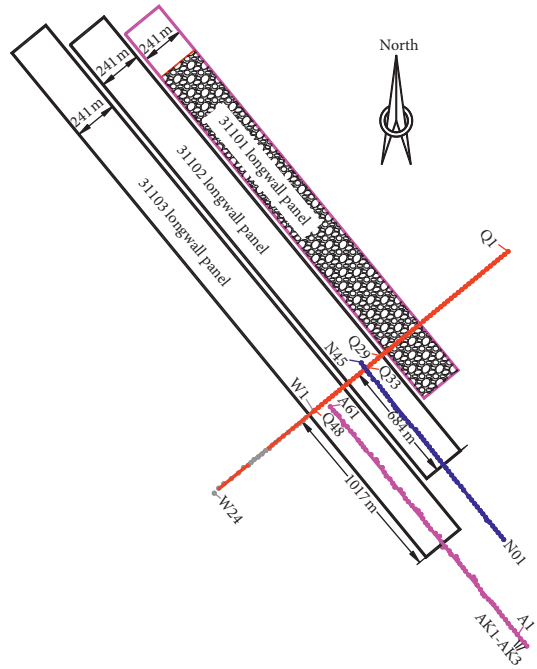

Figure 4: Monitoring lines above the panels.

Table 1: Detailed information about the monitoring lines.

Line name	Length (m)	Point no.	Monitoring period	Note
Line N	1270	N01–N45	11/21/2017–10/24/2018	In the middle of 31102 panel along strike across the setup room
Line A	1670	AK1–AK3 and A1–A61	7/27/2019–7/5/2020	In the middle of 31103 panel along strike across the setup room
Line Q	2276	KQ1–KQ3, Q1–Q23, Z33, Q25–Q48, W1–W20, and K1–K3	11/21/2017–7/3/2020	Along the dip of 31102 and 31103 panels near the setup room

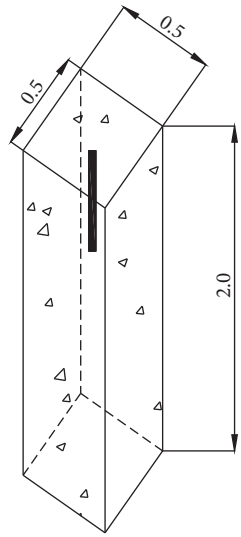

Figure 5: Schematic of the survey peg at each point.

Table 2: Monitoring times for Line N and the corresponding face advance distances.

Monitoring time	Face advance distance (m)
11/16/2017	825
12/02/2017	932
01/13/2018	1113
02/05/2018	1268
02/11/2018	1306
02/26/2018	1373
03/23/2018	1609
04/10/2018	1776
04/25/2018	1906
05/14/2018	2075
06/10/2018	2302
07/01/2018	2398
07/27/2018	2465
09/12/2018	2635
05/14/2019	3099

As we can see, the subsidence did not cease yet until May 14, 2019, although Point N 45 was 684 m away from the setup room and the face advance was 3099 m. It can be found from the plot that subsidence lagged far behind the panel extraction. Although the thickness of the coal seam is 5.5 m, after the final extraction of 3099 m of the panel on May 14, 2019, the maximum subsidence was still less than 1.5 m,

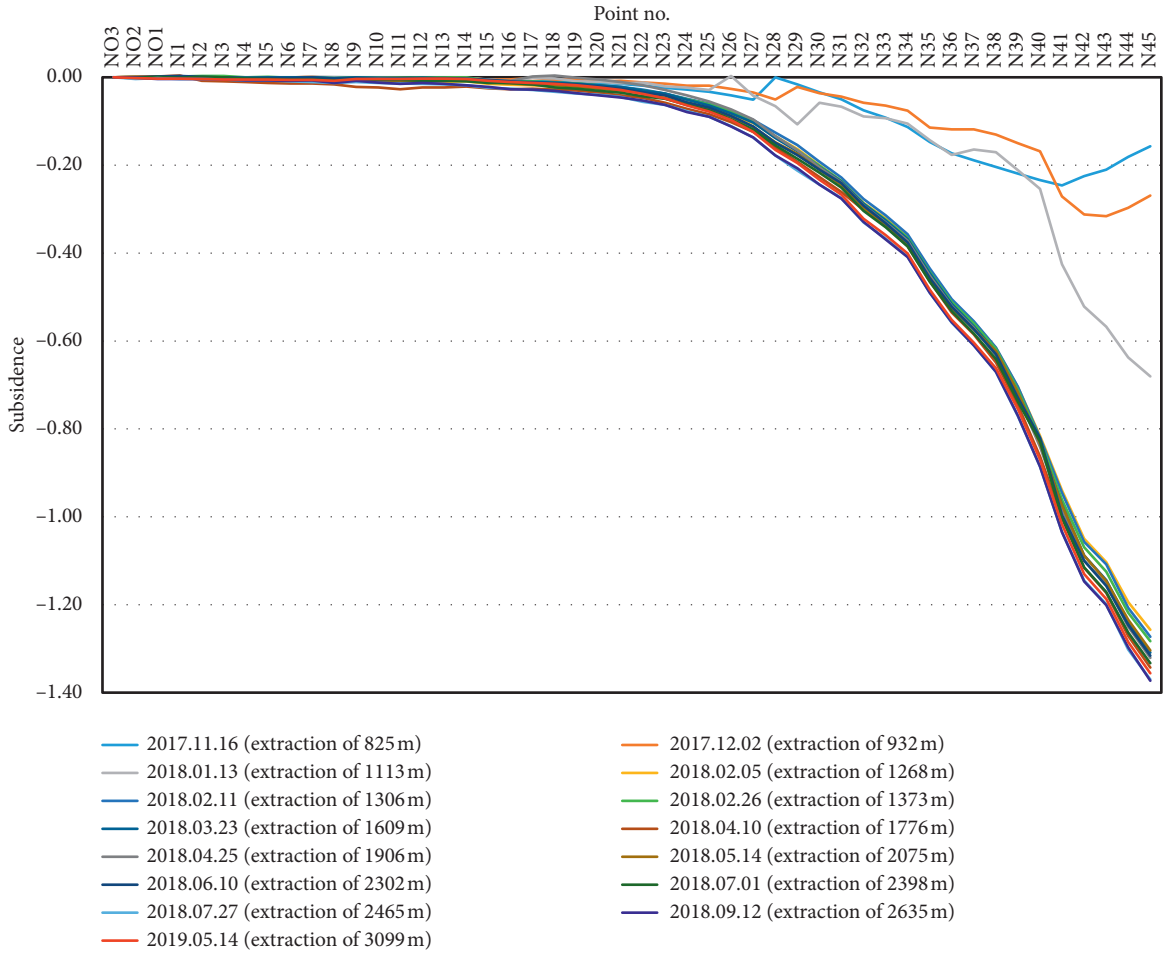

Figure 6: Profile of monitoring Line N along strike of 31102 panel.

which is far from the result of that of critical width of panel extraction.

However, for a period of time of over 8 months from Sep 12, 2018, to May 14, 2019, the subsidence increment of each point was less than 20 mm, that is, less than 2.5 mm per month. This seems to indicate that the subsidence ceased.

The abrupt adjustment of subsidence occurred between Dec 2, 2017, when the face advance was 932 m, and Feb 5, 2018, when the face was 1268 m. The face had already passed Point N 45 by almost 250 m on Dec 2, 2017. During this period of time of 2 months, the subsidence increased over 1 m. Therefore, it is deemed that this was due to the dramatic structural adjustment of masonry broken strata that bridged with the overburden.

Survey for Line Q was conducted 15 times from 11/16/2017 to 5/14/2019 as shown in Table 3. The profile of this line is shown in Figure 7. For comparison, the final subsidence of panel 31101 is presented in Figure 8. As we can see, the maximum subsidence point for 31101 panel is Q 26 with a value of 1.486 m.

Due to the influence of the mined-out 31101 panel, the maximum subsidence point on Line Q was not located in the middle of 31102 panel (see Figure 4, Q33 or Q34); rather, it was Point Q 29 which was about 120 m away from the middle of the panel and located at the chain pillar edge between 31101 and 31102 panels. The maximum subsidence value of Point Q 29 was 2.27 m. It is also noted that the profiles of all the curves did not present a flat-bottomed characteristic; that is, supercritical subsidence basin did not

Table 3: Monitoring times for Line Q and the corresponding face advance distances.

Monitoring time	Face advance distance (m)
11/21/2017	856
12/07/2017	965
12/16/2017	965
02/05/2018	1268
01/12/2018	1107
01/20/2018	1164
02/03/2018	1255
02/22/2018	1306
03/07/2018	1306
03/22/2018	1487
04/08/2018	1760
04/24/2018	1898
05/16/2018	2085
06/12/2018	2317
10/24/2018	2827

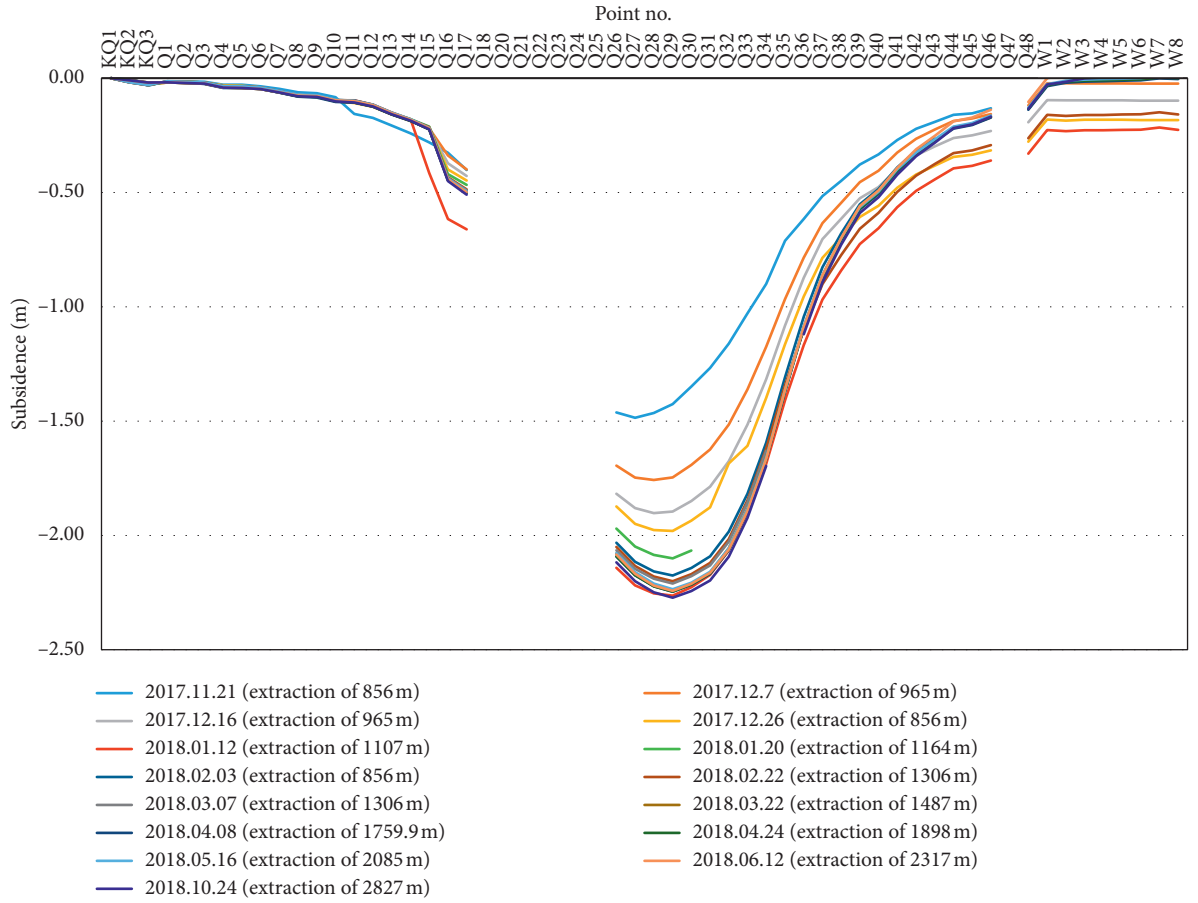

Figure 7: Profile of monitoring Line Q along the dip of 31102 panel.

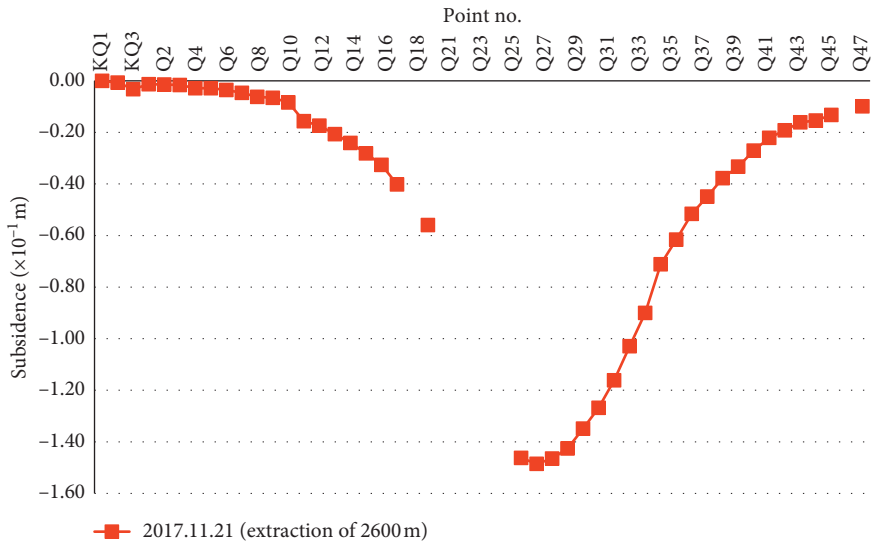

Figure 8: Profile of Line Q along the dip of 31101 panel.

develop. Therefore, despite the panel width of 241 m, it is concluded that the critical panel width was not reached. This also suggests that a 20 m of chain pillar between the two panels does not have an obvious influence on surface subsidence because there was no wavy surface subsidence.

Survey of Line A was conducted for a long period from 7/27/2019 to 7/5/2020. The details of survey times and corresponding face advance distances are given in Table 4. 22 groups of data were collected. The profile of this line based on the data is shown in Figure 9.

Table 4: Monitoring time for Line A and the corresponding working face advance distances.

Time	7/27/2019	8/16/2019	8/31/2019	9/15/2019	9/30/2019
Face advance distance/m	553 m	696 m	746 m	772 m	789 m
Time	2019.10.17	2019.10.27	2019.11.4	2019.11.13	2019.11.20
Face advance distance/m	810 m	827 m	850 m	850 m	850 m
Time	2019.11.27	2019.12.8	2019.12.19	2019.12.28	2020.02.27
Face advance distance/m	881	916	945	977	1084 m
Time	2020.03.17	2020.04.26	2020.05.09	2020.06.01	2020.06.18
Face advance distance/m	1132 m	1132 m	1370 m	1478 m	1567 m
Time	2020.07.05				
Face advance distance/m	1657 m				

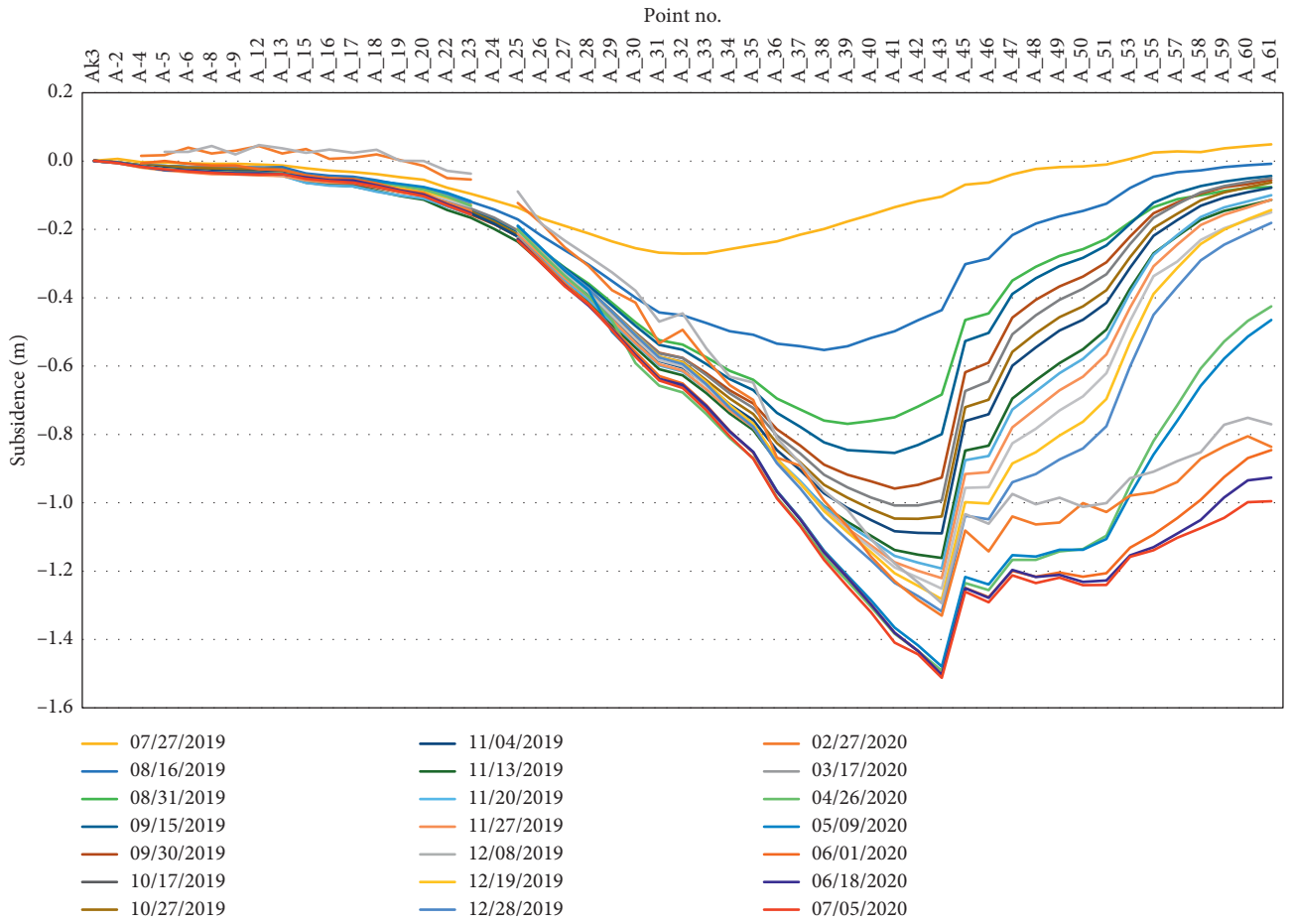

Figure 9: Profile of monitoring Line A along strike of 31103 panel.

It shows that the profiles after 08/16/2019 stayed similar. This indicates that the structures were formed within the overburden strata. The profiles of ground surface are dominated and manifested by the subsurface strata structures [24]. In other words, the profile of the ground surface is representative of the unseen structures within the subsurface strata. The profiles after 08/16/2019 only slightly changed. The subsidence value increased with time but the profiles stayed still similar, and even most parts of profiles after 04/26/2020 were overlapped from what time the subsidence had slowed down significantly after a big adjustment. We can deduce from the change of the profiles that the structures of the overburden strata hardly changed or may be only adjusted slightly. The subsidence magnitude of each point increased while still remaining the profile that first appeared on 08/16/2019.

Extraction of 31102 panel started from 4/1/2020. In order to eliminate the influence of extraction of 31102 panel on subsidence analysis of single 31103 panel, a group of data on 3/17/2020 was chosen for curve fitting as shown in Figure 10. It shows that the maximum subsidence point was A43. The subsidence value and rate were given in Table 5. The subsidence rate of the point is presented in Figure 11(a), and the subsidence value of the point is presented in Figure 11(b).

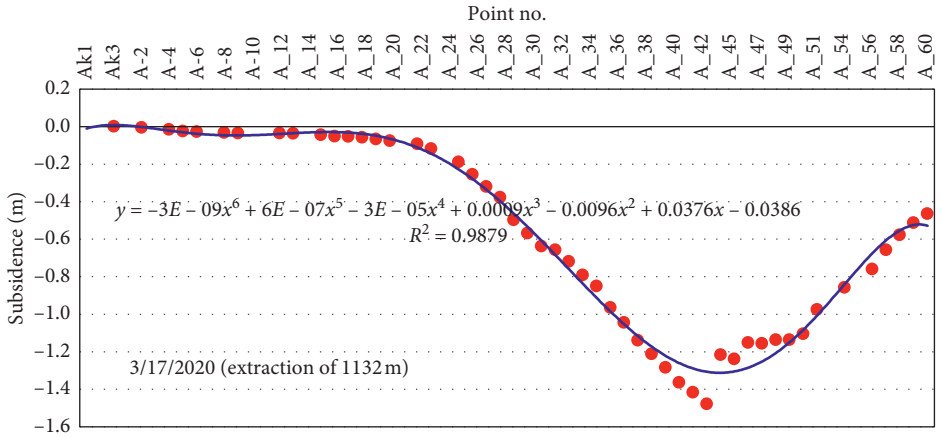

Figure 10: Profile of data of 4/1/2020 of 31103 panel and a fit curve to it.

Table 5: Subsidence rate of point A43.

Monitoring time	Subsidence value with respect to survey of last time (mm)	Days from last survey (days)	Rate (mm/d)	Total subsidence (m)
7/27/2019	−104	84	−1.238	−0.104
8/16/2019	−332	20	−16.6	−0.436
8/31/2019	−247	15	−16.467	−0.683
9/15/2019	−116	15	−7.733	−0.799
9/30/2019	−127	15	−8.467	−0.926
10/17/2019	−67	17	−3.941	−0.993
10/27/2019	−47	10	−4.7	−1.04
11/4/2019	−49	8	−6.125	−1.089
11/13/2019	−72	9	−8	−1.161
11/20/2019	−31	7	−4.429	−1.192
11/27/2019	−116	7	−16.571	−1.22
12/8/2019	−31	11	−2.818	−1.251
12/19/2019	−31	11	−2.818	−1.282
12/28/2019	−36	9	−4	−1.318
2/27/2020	−173	61	−2.836	−1.491
3/17/2020	12	19	0.632	−1.479
4/26/2020	−24	40	−0.6	−1.503
5/9/2020	0	13	0	−1.503
6/1/2020	−9	23	−0.391	−1.512
6/18/2020	182	17	10.706	−1.33
7/5/2020	37	17	2.176	−1.294

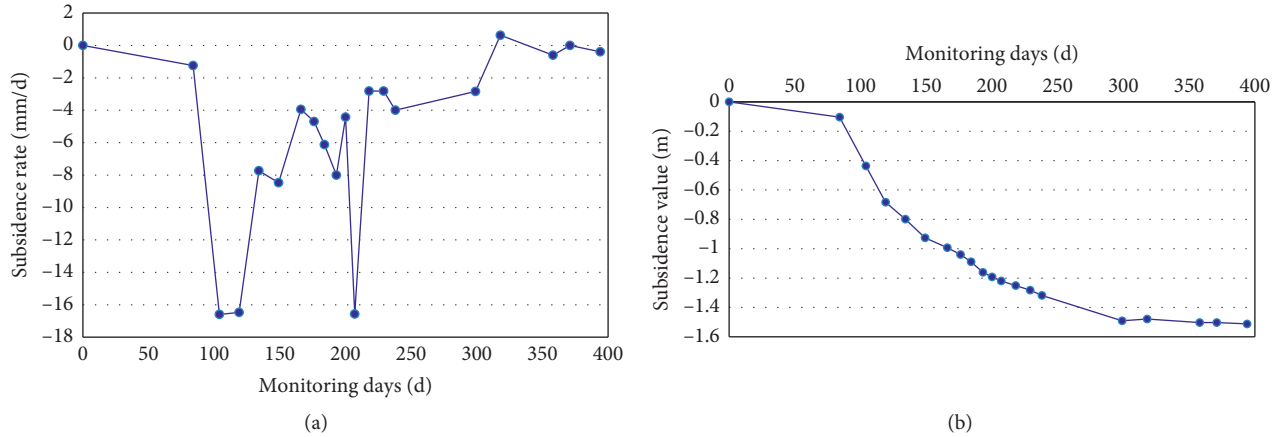

Figure 11: Subsidence data of point A43. (a) The subsidence rate of point A43. (b) The subsidence value of point A43.

The data and figures show that, despite the large face advance distance of 1657 m, however, the ground movement still did not cease, because the coal seam averages about 5.5 m, but the maximum subsidence now was only 1.52 m. From the subsidence rate of point A43, it is demonstrated that subsidence was becoming slower and slower as time went by. Nevertheless, subsidence is going to last for a long time and in some cases, over ten years before the final subsidence is achieved. This phenomenon indicates that the land reuse above underground coal mines should be carefully planned making sure that no potential secondary subsidence occurs in the future, especially sudden and violent future subsidence.

Monitoring for Line Q started from 7/27/2019; 22 groups of data were collected by 7/5/2020. The detail of the survey time and the corresponding face advance distance are shown in Table 6. The profile of the line is presented in Figure 12.

Figure 12 is the profile of Line Q in the dip direction, while Figure 8 is the profile of Line A in the strike direction. Comparing the two figures, it is noticed that the maximum subsidence values of the two monitoring lines for one panel are of great difference. The maximum subsidence of Line Q is 2.74 m while that of Line A is 1.52 m. The reason for this is that the structures formed by the overburden strata are different along both the strike direction and dip direction. For example, the subsidence profile of Line Q must be different from another line parallel to but away from it.

Figure 12 also indicates that there must be twice significant strata structure adjustments within the overburden. One is around 04/29/2020 near point Q44; the other one is around 06/17/2020 near point Q 40. But please note that the location of the strata structure adjustment is not vertically corresponding to the surface point. It is known that there is an area of influence on the surface subsidence due to mining.

The plot also demonstrates that the maximum subsidence point is located in the middle of 31102 panel from Point Q28 to Point Q34 meaning that the chain pillars between the three panels did not have a symptomatic impact on surface subsidence. This may indicate that the 20 m of chain pillars had already been crushed and did not have any function in supporting the overburden strata.

In order to determine the maximum subsidence when the ground surface hardly moved, a group of data on 07/03/2020 was chosen for curve fitting as shown in Figure 12. It shows that the maximum subsidence point is Q32, with a little increase from Points Q28 to Q34. This more or less indicates a characteristic of supercritical subsidence basin. However, the mining height is 5.5 m; the maximum subsidence value is only 2.74. And 2.74/5.5 = 49.8%. In other words, only 49.8% of the maximum possible subsidence was achieved. This indicates that the combined width of the adjacent three panels was far from critical width. But considering the flat-bottomed depression from the profile, it is more likely that the final subsidence is still to come in the future.

The subsidence velocities of the point at different times are presented in Table 7 and the corresponding figure with fitted curve is shown in Figure 13. The subsidence magnitude with respect to time is presented in Figure 14. The inference that can be drawn for explaining the subsidence is given in Figure 15.

Table 6: Survey time and the corresponding face advance distance.

Time	Advance distance (m)
2019/7/27	553
2019/8/29	740
2020/2/29	1084
2020/4/2	1204
2020/4/29	1324
2020/5/13	1395
2020/6/3	1488
2020/6/17	1561
2020/7/3	1567

It is revealed by the data and figures that the stability of strata structures within overburden before the final subsidence controls the profile of the ground surface. As caving of roof strata is bulking controlled process, the compaction of the caved zone is critical for stability evaluation of the ground surface. If the subsidence is complete which means that there is no chance for potential future subsidence, then it is safe to reuse the land. For the case study coal mine, the surface land above the panels is not safe for reuse at the moment and one or two years ahead.

5. Numerical Modelling Study and Discussion

Due to the limitation of the number and the density of monitoring points on the ground surface in the field study, it was impossible to take a more detailed look at the strata movement. Therefore, a numerical modelling study was carried out in which any point in the model can be monitored. As the panel length or advance distance, to be more precise, is significantly larger than panel width, the width is the controlling factor on surface subsidence profile. Therefore, the extraction of the three panels, that is, 31101, 31102, and 31103 panels, in the dip direction was simulated. The constructed model is given in Figure 16. Finer zone resolution in the vicinity of the material boundaries was used. The side boundaries were roller constrained, and the bottom boundary was fixed both horizontally and vertically. Mohr-Coulomb criterion was used to determine the failure of the rock groups. The rock mass engineering parameters were developed based on laboratory tests, supplemented by geologic data and field observation. Then by trial and error, the original parameters were modified slightly by comparing the field subsidence data with the simulated data. The calibrated parameters used for numerical modelling are given in Table 8.

As shown in Figure 8, the monitored maximum subsidence of 31101 panel is 0.15 m. The numerical simulation result is 0.21 m (see Figure 17). The simulated result and the monitored result are in good agreement with each other. After extraction of the 31101 and 31102 panels, as shown in Figure 18, the monitored maximum subsidence in Figure 7 is 2.27 m, and simulated result in Figure 18 is 2.58 m. This result is believed to be reliable. In numerical modelling, the result is obtained when the calculation is totally completed;

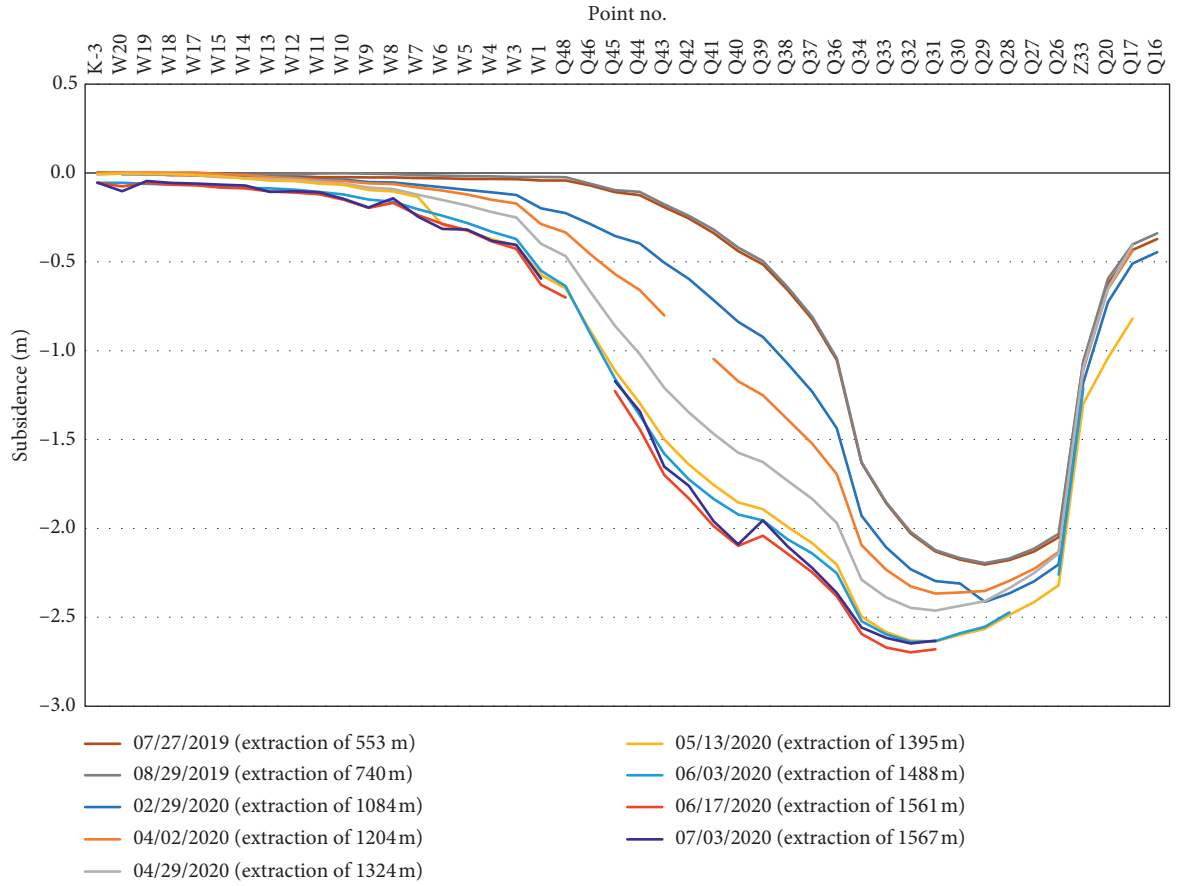

Figure 12: Profile of Line Q along the dip of 31102 panel.

Table 7: Subsidence velocity of point Q32.

Monitoring time	Subsidence value with respect to survey of last time (mm)	Days from last survey (days)	Rate (mm/d)	Total subsidence (m)	Monitoring time
2019/7/27	−2.028	84	−24.143	84	−2.028
2019/8/29	0.008	33	0.242	117	−2.02
2020/2/29	−0.21	184	−1.141	301	−2.23
2020/4/2	−0.096	33	−2.909	334	−2.326
2020/4/29	−0.12	27	−4.444	361	−2.446
2020/5/13	−0.185	14	−13.214	375	−2.631
2020/6/3	−0.007	21	−0.333	396	−2.638
2020/6/17	−0.059	14	−4.214	410	−2.697
2020/7/3	0.05	16	3.125	426	−2.647

that is, the state of equilibrium of the whole model is reached. However, in the field, the subsidence is still not settled completely. Therefore, the slight deviation is normal and the result from the numerical modelling is expected to be slightly larger than the monitored value. The numerical modelling result demonstrates that the pillar between the two panels has no influence on surface subsidence. The field measurement also demonstrates no pillar influence on the surface subsidence. Please also note that both field measurement and numerical modelling do not see the maximum possible subsidence at the center of the trough meaning that the critical width of extraction is not reached even though the adjacent two longwall panels are extracted with a 20 m of pillar left in between. This may be due to the large panel depth of over 600 m.

Figure 19 shows that the simulated maximum subsidence after extraction of the adjacent three panels is 3.92 m. The field monitored result is only 2.72 m (see Figure 12). This result is also believed to be reasonable although the simulated result is much larger than field data because the field data was updated on July 03, 2020. But the subsidence is expected to be totally settled in 1 or 2 or more years. Also, the pillars do not have an obvious effect on the surface subsidence profile. It is noticed that a flat-bottomed depression

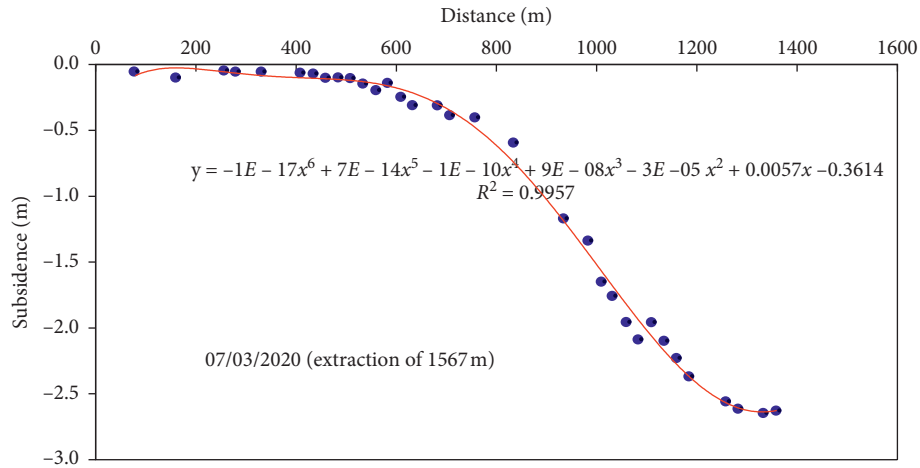

Figure 13: Subsidence value with fitted curve of point Q32.

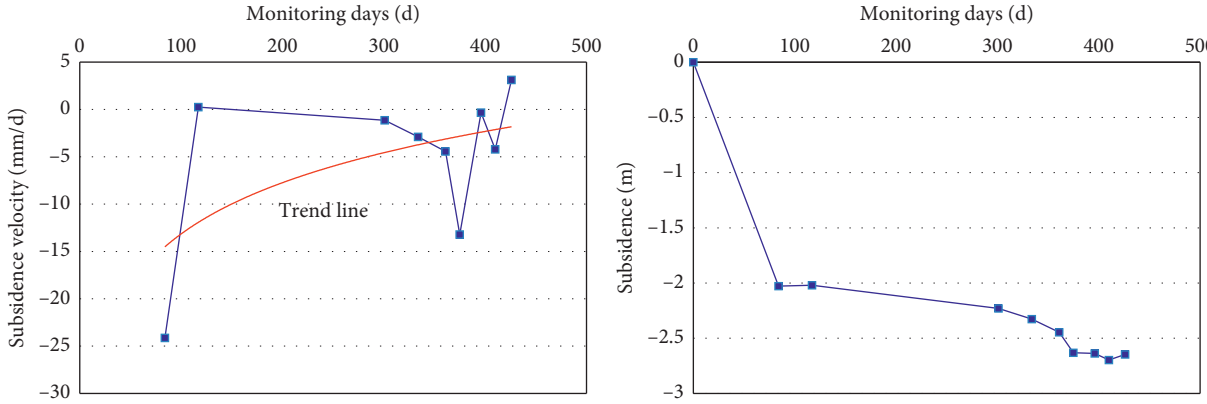

Figure 14: The subsidence velocities and magnitude with respect to time.

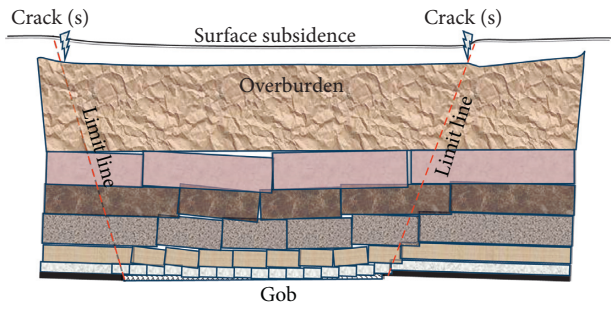

Figure 15: The inference for explaining the control effect of strata structures on subsidence.

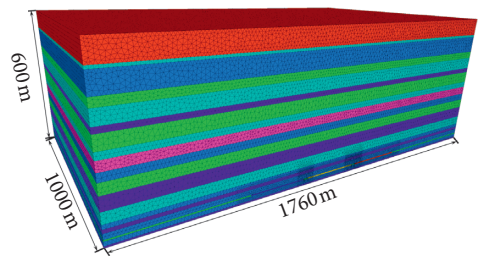

Figure 16: Constructed FLAC3D model.

occurs in both numerical modelling and the field meaning that a supercritical width of extraction is reached. In the numerical modelling, the flat-bottomed trough is about 270 m; in the field, it is about 240 m from points Q26 to Q36 (see Figure 12). The results match well.

Figures 20–22 show the strain increments after extraction of 31101, 31102, and 31103 panels sequentially. Strain increments (Figure 20) indicate that the failure of rock strata penetrates from the edge of 31101 panel and propagates upwards in a shape of trumpet flower (two blue ovals). But the obvious propagation stops at about 245 m above the coal seam. This suggests that the extraction of the 31101 panel does not have a significant influence on the surface subsidence. However, after 31101 and 31102 panels were extracted as shown in Figure 21, the zones of strain increment extend both vertically and transversely within overburden strata and start from the gob edges. The vertical strain increments extend all the way to the surface. This finding is consistent with the field observation that some cracks were found on the boundary of the subsidence trough. After extraction of the three panels as shown in Figure 22, the area of the two strain increment zones highlighted in closed blue lines expands substantially compared with that after extraction of the panels. Many studies indicated that width-to-depth

Table 8: Parameters used for strata.

Lithology	Thickness (m)	Elastic modulus (GPa)	Shear modulus (GPa)	Compressive strength (MPa)	Cohesion (MPa)	Friction angle (°)	Density (kg/m^3)
Alluvium	73.4	0.5	0.3	0.2	0.1	28.0	2500
Fine sandstone	9.6	11.5	6.8	35.0	3.5	38.0	2540
Siltstone	40.3	9.0	5.8	27.0	3.0	37.0	2520
Fine sandstone	70.4	11.5	6.8	35.0	3.5	38.0	2540
Sandy mudstone	29.6	8.0	5.5	15.5	2.5	35.5	2510
Siltstone	51.1	9.0	5.8	27.0	3.0	37.0	2520
Fine sandstone	18.9	11.5	6.8	35.0	3.5	38.0	2540
Sandy mudstone	49.7	8.0	5.5	15.5	2.5	35.5	2510
Siltstone	25.3	9.0	5.8	27.0	3.0	37.0	2520
Fine sandstone	34.0	11.5	6.8	35.0	3.5	38.0	2540
Sandy mudstone	31.0	8.0	5.5	15.5	2.5	35.5	2510
Fine sandstone	41.8	11.5	6.8	35.0	3.5	38.0	2540
Sandy mudstone	48.2	8.0	5.5	15.5	2.5	35.5	2510
Siltstone	40.3	9.0	5.8	27.0	3.0	37.0	2520
Sandy mudstone	15.6	8.0	5.5	15.5	2.5	35.5	2510
Fine sandstone	13.6	11.5	6.8	35.0	3.5	38.0	2540
Sandy mudstone	20.1	8.0	5.5	15.5	2.5	35.5	2510
Coal seam	5.5	4.9	3.1	8.5	1.2	29.2	1400
Sandy mudstone	15.3	8.0	5.5	15.5	2.5	35.5	2510
Fine sandstone	6.6	11.5	6.8	35.0	3.5	38.0	2540

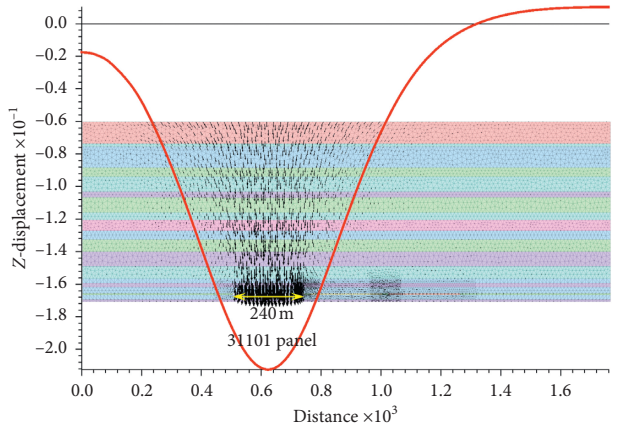

Figure 17: Subsidence of 31101 panel.

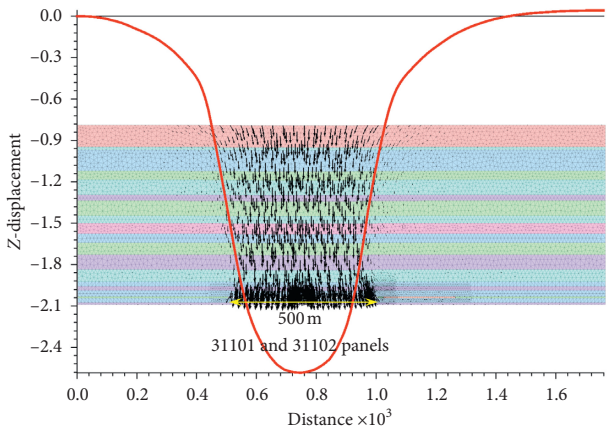

Figure 18: Subsidence of 31101 and 31102 panels.

ratios of extraction are the factor for evaluating whether the critical width of the extraction is reached. Compared with Figure 19, it is also concluded that, after extraction of the three panels, the critical width of extraction is about to be reached. This is in good agreement with many other researchers' studies that panel width-to-depth ratio of 1.2 is the critical value for the occurrence of critical width of extraction supported by a wide range of surface subsidence data worldwide (Figure 23). If the influence of chain pillars between panels is ignored (Figure 24 also shows that the pillars are completely crushed meaning that they have no significant supporting influence or function), then the width-to-depth ratio of extraction of the three panels is 760/600, equaling 1.27, which is slightly larger than 1.2. As we can see from the figures, the subsidence trough is more or less flat-bottomed although the proportion of the flat bottom

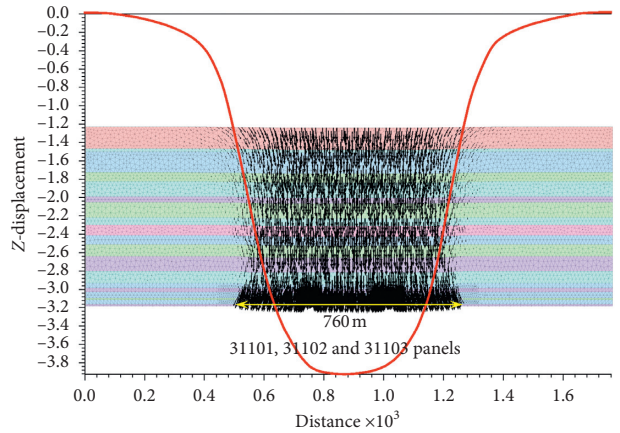

Figure 19: Subsidence of 31101, 31102, and 31103 panels.

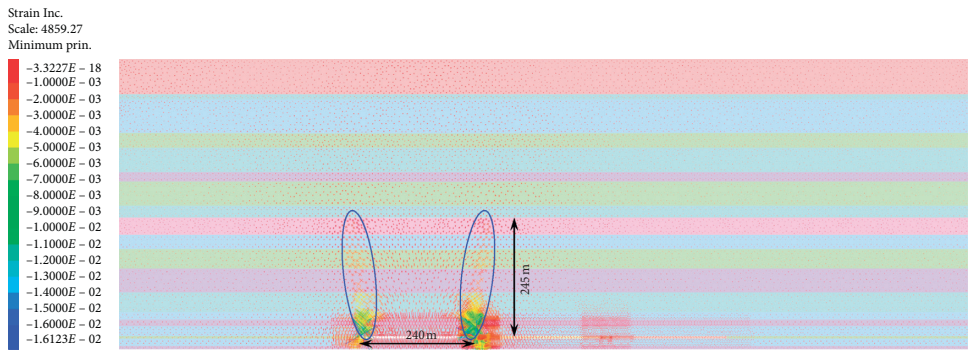

Figure 20: Strain increments of strata after extraction of 31101 panel.

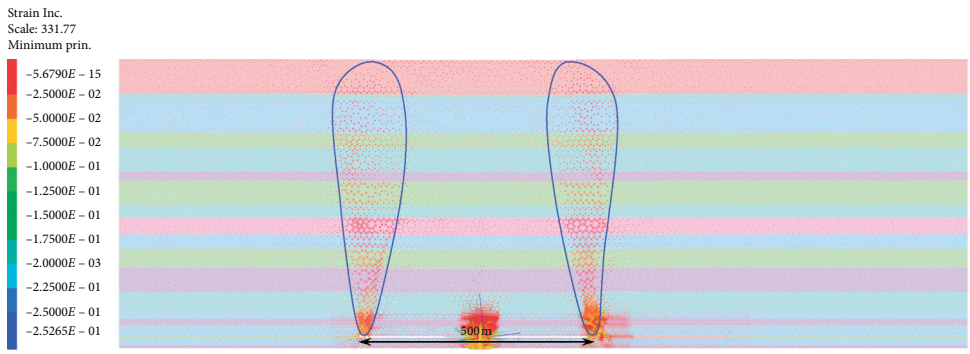

Figure 21: Strain increments of strata after extraction of 31101 and 31102 panels.

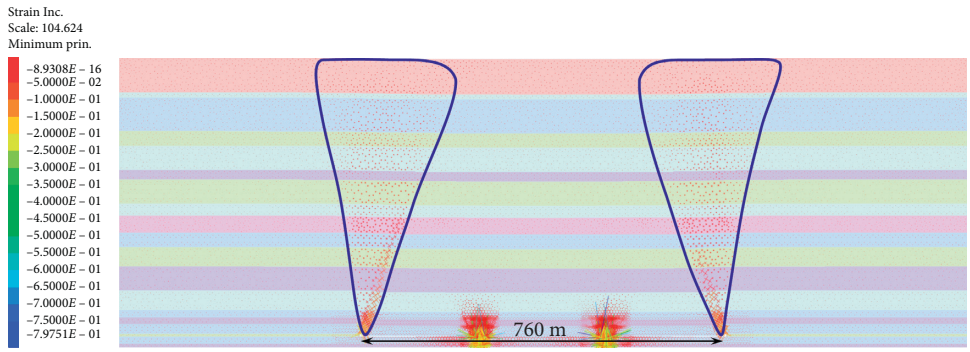

Figure 22: Strain increments of strata after extraction of 31101, 31102, and 31103 panels.

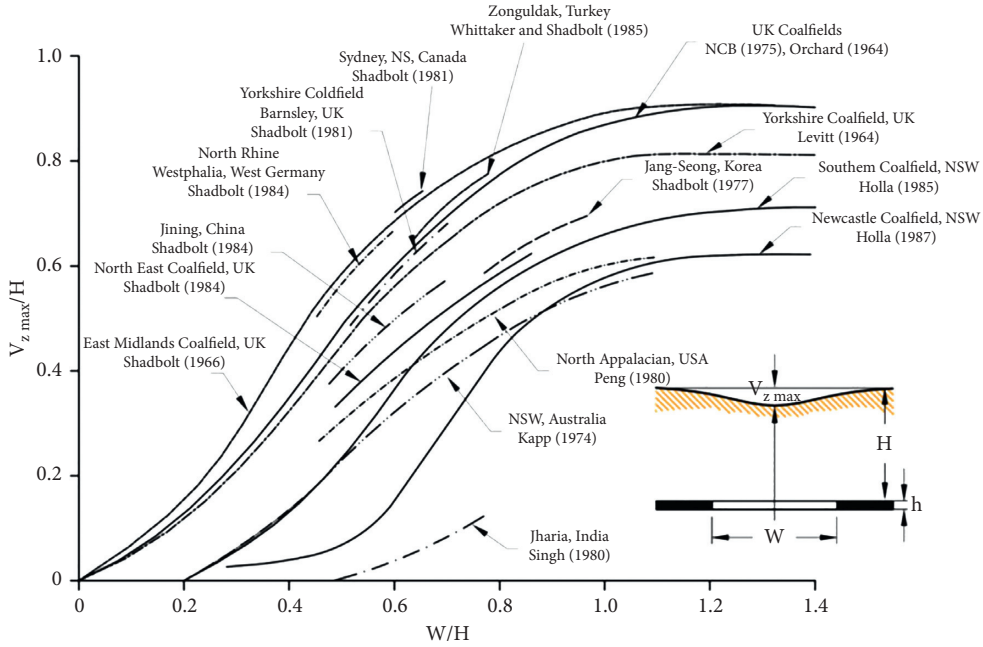

Figure 23: Influence of width-to-depth ratio on maximum vertical surface subsidence [25].

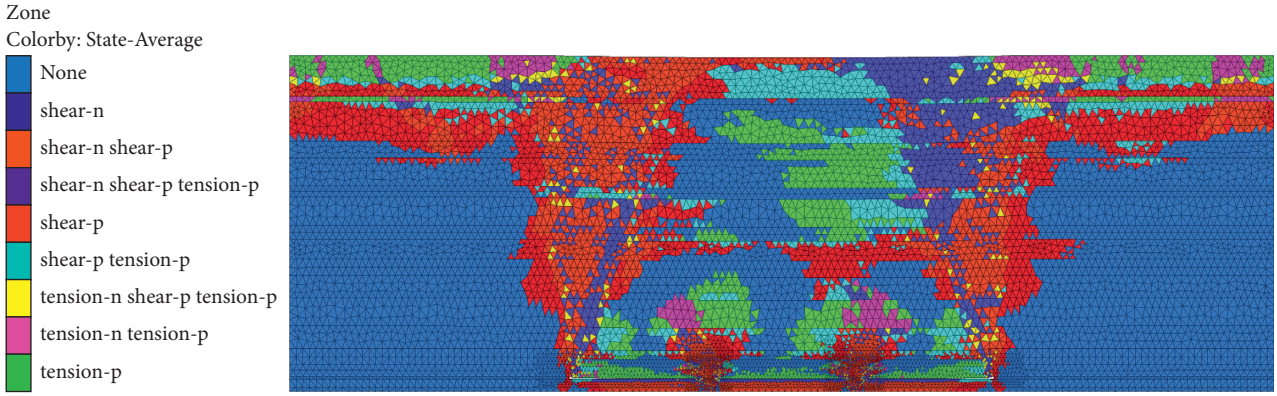

Figure 24: Yield state of rock mass.

is rather small and the simulated maximum subsidence after extraction of 31103 panel is 3.92 out of 5.5 m (71.3%).

All in all, the numerical modelling results are generally in good agreement with field monitoring results. Please note that FLAC3D which is a finite difference software was used for numerical modelling study. As a result, caving or surface cracks or structural formed by the overburden strata cannot be modelled explicitly. However, the advantage of the software is that the subsidence value of any point in the model can be monitored; it is more applicable for continuous and uniform subsidence with small subsidence values. For other geological conditions where large subsidence or cracks occur, UDEC or other types of similar software are better.

6. Conclusions

A field measurement and numerical study on mining-induced subsidence of three adjacent longwall panels in a coal mine in Northwest China is presented in this study. The panels are 241 m wide and over 3000 m long extracting a coal seam of 5.5 m thick.

It is found that surface subsidence lags far behind panel extraction or mining activity. The profiles of ground surface are dominated and manifested by the subsurface strata structures. Structures formed by the overburden strata are different along both strike direction and dip direction. As a result, the subsidence influence throughout the whole length of a longwall panel varies. Dramatic adjustment of strata structures may induce violent surface subsidence. Stability of strata structures within overburden before the final subsidence controls the stability of ground surface land. Chain pillars of 20 m between panels of 240 m wide with a cover depth of 600 m have been crushed in the gob and do not have any function in supporting the overburden strata.

The study also suggests that the final subsidence of the three adjacent panels is far to come in the future, and the land reuse above underground coal mines should be

carefully planned by making sure that the gob is completely compacted or no potential secondary subsidence occurs in the future.

It is hoped that the investigations of this study can provide some insight into taking positive measures for environmental protection and land reuse plan for post-mining cities.

Data Availability

The data used to support the findings of this study are available upon request.

Conflicts of Interest

The authors declare no conflicts of interest.

Authors' Contributions

Kai Zhang contributed to conceptualization and supervision; Lu Bai and Pengfei Wang performed formal analysis, investigation, and data curation; wrote the original draft; provided the software; and reviewed and edited the article; Zhuang Zhu checked typos and grammatical errors; Kai Zhang contributed to funding acquisition.

Acknowledgments

This work was cosupported by the Research on Ecological Restoration and Protection of Coal Base in Arid Eco-Fragile Region (GJNY2030XDXM-19-03.2), the National Key Research and Development Program of China (2018YFC0406404), the Yue Qi Young Scholar Project, China University of Mining & Technology, Beijing (2019QN08), the Fundamental Research Funds for the Central Universities (2020YJSHH12), the National Natural Science Foundation of China (52004012), and Funds for Talents Supported by China Association for Science and Technology and Shanxi Science and Technology Major Project (20201101009).

References

[1] Q. Zeng, L. Shen, and J. Yang, "Potential impacts of mining of super-thick coal seam on the local environment in arid Eastern Junggar coalfield, Xinjiang region, China," *Environmental Earth Sciences*, vol. 79, no. 4, p. 88, 2020.

[2] J. Białek, M. Wesołowski, R. Mielimąka, and P. Sikora, "Deformations of mining terrain caused by the partial exploitation in the aspect of measurements and numerical modeling," *Sustainability*, vol. 12, p. 5072, 2020.

[3] Y. Zhang, S. Cao, R. Gao, S. Guo, and L. Lan, "Prediction of the heights of the water-conducting fracture zone in the overlying strata of shortwall block mining beneath aquifers in western China," *Sustainability*, vol. 10, no. 5, p. 1636, 2018.

[4] V. D. J. Roosendaal, *Longwall Mine Subsidence of Farmland in Southern Illinois: Near-Surface Fracturing and Associated Hydrogeological Effects: Proceeding of 1992 National Symposium on Prime Farmland Reclamation*, University of Illinois Press, Champaign, IL, USA, 1992.

[5] D. E. Seils, R. G. Darmody, and F. W. Simmons, *The Effects of Coal Mine Subsidence on Soil Macroporsity and Water Flow: Proceeding of 1992 National Symposium on Prime Farmland Reclamation*, University of Illinois Press, Urbana, 1992.

[6] C. J. Booth, E. D. Spande, C. T. Pattee, J. D. Miller, and L. P. Bertsch, "Positive and negative impacts of longwall mine subsidence on a sandstone aquifer," *Environmental Geology*, vol. 34, no. 2-3, pp. 223–233, 1998.

[7] C. J. Booth, "Groundwater as an environmental constraint of longwall coal mining," *Environmental Geology*, vol. 49, no. 6, pp. 796–803, 2006.

[8] K.-D. Kim, S. Lee, H.-J. Oh, J.-K. Choi, and J.-S. Won, "Assessment of ground subsidence hazard near an abandoned underground coal mine using GIS," *Environmental Geology*, vol. 50, no. 8, pp. 1183–1191, 2006.

[9] Y. Li, "Groundwater system for the periods of pre- and post-longwall mining over thin overburden," *International Journal of Mining, Reclamation and Environment*, vol. 30, no. 4, pp. 295–311, 2016.

[10] J. Cheng, G. Zhao, G. Feng, and S. Li, "Characterizing strata deformation over coal pillar system in longwall panels by using subsurface subsidence prediction model," *European Journal of Environmental and Civil Engineering*, vol. 24, no. 5, pp. 650–669, 2020.

[11] G. Marino, A. Osouli, M. Elgendy, and M. Karimpour, "Utilization of historical subsidence data for prediction of adverse subsidence conditions over trona mine," *International Journal of Geomechanics*, vol. 17, no. 2, 2016.

[12] P. Shi, Y. Zhang, Z. Hu, K. Ma, H. Wang, and T. Chai, "The response of soil bacterial communities to mining subsidence in the west China aeolian sand area," *Applied Soil Ecology*, vol. 121, pp. 1–10, 2017.

[13] Z. Yang, J. Li, C. E. Zipper, Y. Shen, H. Miao, and P. F. Donovan, "Identification of the disturbance and trajectory types in mining areas using multitemporal remote sensing images," *Science of The Total Environment*, vol. 644, pp. 916–927, 2018.

[14] A. Guney and M. Gul, "Analysis of surface subsidence due to longwall mining under weak geological conditions: turgut basin of Yatağan-Muğla (Turkey) case study," *International Journal of Mining, Reclamation and Environment*, vol. 33, no. 7, pp. 445–461, 2019.

[15] K. Ma, Y. Zhang, M. Ruan, J. Guo, and T. Chai, "Land subsidence in a coal mining area reduced soil fertility and led to soil degradation in arid and semi-arid regions," *International Journal of Environmental Research and Public Health*, vol. 16, no. 20, p. 3929, 2019.

[16] D. P. Marian, I. Onica, R.-R. Marian, and D.-A. Floarea, "Finite element analysis of the state of stresses on the structures of buildings influenced by underground mining of hard coal seams in the jiu valley basin (Romania)," *Sustainability*, vol. 12, no. 4, p. 1598, 2020.

[17] A. Dawkins, "Potential management and rehabilitation requirements of environmental effects from longwall subsidence on streams, lakes and groundwater systems," in *Proceedings of the Coal 2003: Coal Operators Conference*, pp. 117–124, Wollongong, Australia, February 2003.

[18] M. R. Haibach, B. Benson, J. Silvis et al., "Mitigation techniques for mine subsidence impacts on streams," *Coal News*, vol. 9, p. 32, 2012.

[19] Z. Hu and W. Xiao, "Optimization of concurrent mining and reclamation plans for single coal seam: a case study in northern Anhui, China," *Environmental Earth Sciences*, vol. 68, no. 5, pp. 1247–1254, 2013.

[20] Y. Li, L. Chen, H. Wen, T. Zhou, T. Zhang, and X. Gao, "Pyrosequencing analysis of bacterial diversity revealed by a comparative study of soils from mining subsidence and reclamation areas," *Journal of Microbiology and Biotechnology*, vol. 454, no. 24, pp. 313–323, 2014.

[21] S. Wang, X. Li, and S. Wang, "Separation and fracturing in overlying strata disturbed by longwall mining in a mineral deposit seam," *Engineering Geology*, vol. 226, pp. 257–266, 2017.

[22] Y. Bi, J. Zhang, Z. Song et al., "Arbuscular mycorrhizal fungi alleviate root damage stress induced by simulated coal mining subsidence ground fissures," *Science of the Total Environment*, vol. 652, pp. 398–405, 2019.

[23] X. Y. Wang, Y. Li, Y. Wei et al., "Effects of fertilization and reclamation time on soil bacterial communities in coal mining subsidence areas," *Science of the Total Environment*, vol. 739, Article ID 139882, 2020.

[24] G. Feng and P. Wang, "Simulation of recovery of upper remnant coal pillar while mining the ultra-close lower panel using longwall top coal caving," *International Journal of Mining Science and Technology*, vol. 30, no. 1, pp. 55–61, 2020.

[25] J. M. Galvin, *Ground Engineering: Principles and Practices for Underground Coal Mining*, pp. 92-93, Springer, Cham, Switzerland, 2016.